Biometrical Journal **44** (2002) 6, 718–745

Two-Dimensional Spectral Analysis for Marked Point Processes

ERIC RENSHAW*

Department of Statistics and Modelling Science, Strathclyde University, Livingstone Tower, 26 Richmond Street, Glasgow G1 1XH, United Kingdom

Summary

Spectral analysis has already been shown to be a powerful tool in the interrogation of lattice patterns, since it assumes no structural characteristics in the data (such as isotropy) prior to analysis. Here we extend the analysis to non-lattice data for which both points and marks can exhibit spatial structure. Both distance- and spectral-based measures are introduced, and theoretical comparisons are made between lattice and mark spectra. Simulated examples suggest a high degree of independence between point and mark spectra, and a real example is presented for the spatial structure of 584 tree locations and diameters at breast height of longleaf pine trees in southern Georgia.

Key words: Anisotropy; Cartesian and polar spectra; Clumping; Competition; Inhibition; Lattice spectra; Longleaf pine; Point and mark spectra; Scales of pattern; Second-order moment functions; Spatial analysis.

1. Introduction

Spatial data fall into two distinct categories, depending on whether they are located at the nodes of a regular lattice or within a continuous region of space. The former generally occur in digitized images, and are often associated with the transmission and processing of signals generated by, for example, satellite, air-reconnaissance and medical cameras. Such lattice-based data are not only easy to handle both graphically and computationally, but they can also be exploited algebraically to yield compact analytic results (e.g. CAPOBIANCO and RENSHAW, 1998 and NEWBERY, RENSHAW, and BRUNIG, 1986). Given these advantages, it is tempting to record observations over a rectangular grid of points even when measurements are being taken of a continuous system comprising marks sited at point locations: mathematical analysis of such marked point patterns is far more complex since we not only lose lattice-based tractability, but also have to contend with three sets of potentially related spatial interaction, namely point-point, point-mark and mark-mark. Although RENSHAW and FORD (1983) show that substantial progress can be made by using a lattice-based approximation, they warn that care is

* Corresponding author: eric@stams.strath.ac.uk

 0323-3847/02/0609-0718 $ 17.50+.50/0

needed to ensure that the covering mesh is sufficiently fine. The purpose of this paper is first to quantify the difference between the continuous and lattice spectral approaches, and then to assess the extent to which the spatial pattern of the marks can be disentangled from that of their associated point locations.

Techniques for dealing with lattice-based observations are well-documented, and generally involve either the autocovariance function (a.c.f.) or the periodogram (i.e. sample spectral function). Whilst the former highlights the underlying wavelengths of spatial pattern, the latter is based on the frequency of pattern repeats; though since the periodogram is the Fourier transform of the a.c.f., and vice-versa, the two functions reveal the same spatial information (PRIESTLEY, 1981), albeit in different ways. The problem is that this extremely useful link does not apply to marked point process (m.p.p.) patterns. Although the early study of m.p.p.'s received some attention in the space-domain literature (e.g. HANISCH and STOYAN, 1979), the claim by STOYAN (1984a) that this was far less than its importance demanded led to considerable development in the covariance approach (see, for example, STOYAN, 1984b; PENTINNEN, STOYAN, and HENTTONEN, 1992; STOYAN, KENDALL, and MECKE, 1987). STOYAN and STOYAN (1994) provide an eminently lucid account which neatly outlines mathematical ideas without presenting formal mathematical proofs. Unfortunately, parallel developments have not occurred in the spectral domain, most likely because when moving from a lattice to continuous space the algebraic simplification which results from summing regularly spaced sines and cosines no longer holds. Although this paper concentrates on the frequency domain, we stress that in practice it is important to investigate all possible approaches if our understanding of pattern structure and process generating mechanism is to be maximized. For an impressively comprehensive, single-source guide to both the theory and applied aspects of spatial statistical methods see CRESSIE (1993); whilst for an introduction to the theory of point processes see DALEY and VERE-JONES (1988).

An excellent example which highlights the marked-point approach is the spatial (and temporal) analysis of earthquake data; the epicentre is the point and the shock magnitude the mark. The excessive spatial inhomogeneity associated with the subduction of interacting plates generates problems of considerable statistical interest, and one way of gaining greater understanding of such seismological events is through the development of likelihood and three-dimensional spline techniques (e.g. OGATA and KATSURA, 1988, 1993; OGATA, IMOTO, and KATSURA, 1991). GOULARD, GRABARNIK, and SÄRKKÄ (1996) discuss the general use of maximum pseudo-likelihood for estimating parameters in marked Gibbs processes; whilst OGATA and TANEMURA (1985) use maximum likelihood to estimate interaction potentials. RENSHAW and SÄRRKÄ (2001) develop purely spatial summary measures, also based on marked Gibbs processes, from which they can infer underlying generating mechanisms of space-time stochastic processes. Work is currently in progress to relate these ideas to continuous space extensions of the lattice-based growth-interaction process studied by RENSHAW (1984) and RENSHAW,

PHAYRE, and JAKEMAN (2000); the latter solves the inverse problem of constructing a space-time process with a designated spectrum, and so provides a direct relationship between spectrum and process.

We define a marked point process to be the paired-set $\{p_i, X_i\}$, where p_i is the location of the ith event with coordinates (x_i, y_i), and X_i is the mark associated with p_i. For a stationary, isotropic process the standard correlation-based approach is to work with the mean product of marks sited a distance r apart, i.e.

$$M(r) = \lambda^2 g(r)\, S(r)\, \mathrm{d}p_1\, \mathrm{d}p_2\,. \tag{1.1}$$

The intensity λ denotes the mean number of events per unit area, $g(r)$ and $S(r)$ denote the (pair) correlation functions for points and marks, respectively, and $\mathrm{d}p_1$ and $\mathrm{d}p_2$ are two infinitesimally small areas separated by a distance r. So for a pure homogeneous Poisson process $g(r) \equiv 1$, whilst for a pure point process $S(r) \equiv 1$. Note that $g(r)$ is related to Ripley's K-function through

$$g(r) = \frac{1}{2\pi r}\,\frac{\mathrm{d}K(r)}{\mathrm{d}r}\,. \tag{1.2}$$

STOYAN and STOYAN (1994) provide an extensive discussion of such functions, together with a natural extension to cover anisotropic processes by replacing (1.1) by the polar form

$$M(r, \theta) = \lambda^2 g(r, \theta)\, S(r, \theta)\, \mathrm{d}p_1\, \mathrm{d}p_2\,, \tag{1.3}$$

where θ denotes the angle between $\mathrm{d}p_1$ and $\mathrm{d}p_2$. This function is extremely useful for analyzing spatial patterns over irregularly-shaped regions; in the associated estimation procedure use of an edge-correction factor (FIKSEL, 1988) eliminates bias caused by those points which lie close to the boundary. However, for mark/point data collected over a rectangular region a Cartesian framework is the natural first choice (e.g. FORD and RENSHAW, 1984), and it allows us to link into known lattice-based results. CAPOBIANCO and RENSHAW (1998) therefore develop a procedure which replaces the polar distance (r, θ) by the Cartesian distance (j, l) through the 'city-block' metric form

$$M(j, l) = \lambda^2 g(j, l)\, S(j, l)\, \mathrm{d}p_1\, \mathrm{d}p_2\,, \tag{1.4}$$

and examine the effect of incorporating two different covariance estimators for $S(j, l)$. These are directly applicable to marked point patterns observed on an $m \times n$ lattice, and so enable us to switch directly between continuous and lattice space. In the latter case we recover the autocovariance estimator discussed by RENSHAW and FORD (1983, 1984) for lattice marks $\{X_{st}\}$ $(s = 1, \ldots, m;\ t = 1, \ldots, n)$, namely

$$C(j, l) = (1/mn) \sum_{s=1}^{m-j} \sum_{\Omega_t} X_{st} X_{s+j,\, t+l}\,, \tag{1.5}$$

where $\Omega_t = \{1, \ldots, n;\ l \geq 0\} \cup \{-l+1, \ldots, n;\ l < 0\}$. Only non-negative values of j need be considered since $C(-j, l) = C(j, -l)$. The associated periodogram (i.e. sample spectral function) $\{I_{pq}\}$ over frequencies $p = 0, \ldots, m/2$, $q = -n/2, \ldots, n/2 - 1$ is then easily constructed via the Fourier cosine transform

$$I_{pq} = \sum_{j=-m+1}^{m-1} \sum_{l=-n+1}^{n-1} C(j, l) \cos\left[(pj/m) + (ql/n)\right]. \tag{1.6}$$

2. The Spectral Approach

The theory for describing the properties of one-dimensional series of events (usually in a temporal context) has been well-described by COX and LEWIS (1966), BRILLINGER (1972), DALEY and VERE-JONES (1972) and Lewis (1972). To extend this to two-dimensions, we could follow BARTLETT's (1964) extension to his one-dimensional spectral theory (BARTLETT, 1963). However, it is preferable to expand BRILLINGER's (1972) definition instead, since his notation makes the requirement for stationarity in Bartlett's definition explicit (see MUGGLESTONE and RENSHAW, 1996). We first need to define the first- and second-order *intensity functions* of the spatial point process, namely

$$\lambda(\underline{a}) = \lim_{|\mathrm{d}\underline{a}| \to 0} \{E[N(\mathrm{d}\underline{a})]/|\mathrm{d}\underline{a}|\} \tag{2.1}$$

and

$$\lambda'(\underline{a}, \underline{b}) = \lim_{|\mathrm{d}\underline{a}|, |\mathrm{d}\underline{b}| \to 0} \{E[N(\mathrm{d}\underline{a})\, N(\mathrm{d}\underline{b})]/|\mathrm{d}\underline{a}|\, |\mathrm{d}\underline{b}|\} \qquad (\underline{a} \neq \underline{b}), \tag{2.2}$$

respectively. Here $\mathrm{d}\underline{a}$ and $\mathrm{d}\underline{b}$ are small regions of the plane, with areas $|\mathrm{d}\underline{a}|$ and $|\mathrm{d}\underline{b}|$, containing the points $\underline{a}$ and $\underline{b}$, whilst $N(\mathrm{d}\underline{a})$ is the number of points in $\mathrm{d}\underline{a}$. The *covariance density function*

$$\gamma(\underline{a}, \underline{b}) = \lambda'(\underline{a}, \underline{b}) - \lambda(\underline{a})\, \lambda(\underline{b}), \tag{2.3}$$

and definitions (2.2) and (2.3) may both be extended to include the case $\underline{a} = \underline{b}$ by assuming that the process is *orderly*, i.e. only one event can occur in a particular point in space. In this situation $E[\{N(\mathrm{d}\underline{a})\}^2] = E[N(\mathrm{d}\underline{a})] = \lambda(\underline{a})\, |\mathrm{d}\underline{a}|$, which leads to BARTLETT's (1964) *complete covariance density function*

$$\kappa(\underline{a}, \underline{b}) = \lambda(\underline{a})\, \delta(\underline{a} - \underline{b}) + \gamma(\underline{a}, \underline{b}), \tag{2.4}$$

where $\delta(x)$ denotes the Dirac delta function. Note that if the process is *stationary* (to second-order), then $\lambda(\underline{a}) \equiv \lambda$ whilst $\lambda'(\underline{a}, \underline{b})$ reduces to $\lambda'(\underline{a} - \underline{b})$.

We can now define the *point spectral density function* as the Fourier transform of $\gamma(\underline{a}, \underline{b})$, namely

$$f(\underline{\omega}_1, \underline{\omega}_2) = \int\int \gamma(\underline{a}, \underline{b}) \exp\{-i(\underline{\omega}_1'\underline{a} + \underline{\omega}_2'\underline{b})\}\, \mathrm{d}\underline{b}\, \mathrm{d}\underline{a}. \tag{2.5}$$

If the process is stationary (to second-order) then $\gamma(\underline{a}, \underline{b})$ depends on $\underline{a}$ and $\underline{b}$ only through $\underline{c} = \underline{a} - \underline{b}$, and for this to hold necessitates $\underline{\omega}_2 = -\underline{\omega}_1$ in (2.5). On writing $f(\underline{\omega}, -\underline{\omega}) \equiv f(\underline{\omega})$ and $\underline{c} = (u, v)$, we then have that for a stationary point process, at frequency $\underline{\omega} = (\omega_1, \omega_2)$,

$$f(\omega_1, \omega_2) = \int_{-\infty}^{\infty} \int_{-\infty}^{\infty} \kappa(u, v) \exp\{-i(\omega_1 u + \omega_2 v)\} \, du \, dv \tag{2.6}$$

with inverse

$$\kappa(u, v) = \int_{-\infty}^{\infty} \int_{-\infty}^{\infty} f(\omega_1, \omega_2) \exp\{+i(\omega_1 u + \omega_2 v)\} \, d\omega_1 \, d\omega_2 \, . \tag{2.7}$$

If the spatial properties of a process are invariant under rotation, i.e. the process is *isotropic*, then the covariance density function is simply a function of r, the scalar distance between the two points $\underline{a}$ and $\underline{b}$. In this case, integrating (2.6) over the phase angle $\tan^{-1}(u/v)$ (BARTLETT, 1964) yields

$$f(\omega_1, \omega_2) \equiv f(\omega) = \lambda + 2\pi \int_0^{\infty} r\gamma(r) \, J_0(r\omega) \, dr \, , \tag{2.8}$$

where $J_0(z)$ is the unmodified Bessel function of the first kind of order zero (WATSON, 1944) and $\omega = \sqrt{(\omega_1^2 + \omega_2^2)}$. The *mark spectral density function* is defined similarly, with $\kappa(u, v)$ being replaced by $M(r)$, $M(r, \theta)$ or $M(j, l)$ depending on whether we are investigating isotropic, polar or city-block forms.

Now whilst (2.6) and (2.8) provide formal definitions of spectral density, we still have to construct the associated estimators. For lattice data we have (1.6), though we can obtain a functionally equivalent representation which is both quicker to compute and less subject to round-off error by evaluating the Fourier coefficients

$$\begin{aligned} A_{pq} &= \sum_{s=1}^{m} \sum_{t=1}^{n} (X_{st} - \bar{X}) \cos[2\pi(ps/m + qt/n)] \, , \\ B_{pq} &= \sum_{s=1}^{m} \sum_{t=1}^{n} (X_{st} - \bar{X}) \sin[2\pi(ps/m + qt/n)] \, , \end{aligned} \tag{2.9}$$

and then forming the lattice periodogram

$$I_{pq}^{L} = (A_{pq}^2 + B_{pq}^2)/mn \, . \tag{2.10}$$

To construct the equivalent m.p.p. structure, suppose that an observed pattern consists of N events contained within a rectangular region of size $L_x \times L_y$, and for notational convenience scale the points $\{(x_i, y_i);\ i = 1, \ldots, N\}$ to lie within the unit square. If the exact values of L_x and L_y are unknown, then (ideally) they should be chosen to ensure that when the rectangle is viewed as a torus the second-order moment structure of nearest-neighbour distances near the (rectangular) boundary is consistent with that in the interior. This prevents anomalous empty

strips at the borders producing spurious low-frequency components in the spectrum. Then on evaluating the Fourier coefficients

$$\begin{aligned} a_{pq} &= \sum_{i=1}^{N} (X_i - \bar{X}) \cos [2\pi(px_i + qy_i)] , \\ b_{pq} &= \sum_{i=1}^{N} (X_i - \bar{X}) \sin [2\pi(px_i + qy_i)] \end{aligned} \tag{2.11}$$

over some appropriate frequency range $p = 0, \ldots, f_x$; $q = -f_y, \ldots, f_y - 1$, the *marked periodogram*

$$I^M_{pq} = (a^2_{pq} + b^2_{pq})/N . \tag{2.12}$$

The *point periodogram* (PRIESTLEY, 1964), I^P_{pq}, is defined similarly, but with $X_i - \bar{X}$ replaced by 1. Here $\bar{X} = \sum X_{st}/mn$ and $\bar{X} = \sum X_i/N$ denote the average lattice and point mark, respectively.

Although the maximum possible frequency for a point process is infinite, since two points can lie arbitrarily close together, in the case of an $m \times n$ lattice there exist maximum (Nyquist) frequencies $p_{\max} = m/2$, $q_{\max} = n/2$. So to compare marked point and lattice spectra we need to take $f_x = m/2, f_y = n/2$ with $N = mn$; the lattice variables $\{X_{st}\}$ translate into the mark variables $\{X_{(s-1)\,n+t}\}$. Now the symmetry of the lattice ensures that $A_{m-p,\,n-q} = A_{pq}$ and $B_{m-p,\,n-q} = B_{pq}$, whence $I^L_{m-p,\,n-q} = I^L_{pq}$. Thus it is only necessary to evaluate the lattice spectrum within the bounded range $p = 0, \ldots, m/2$; $q = -n/2, \ldots, n/2 - 1$. However, for the marked periodogram, no such general Nyquist structure exists, e.g.

$$Na_{2f_x-p,\,2f_y-q} = \sum_{i=1}^{m} X_i \cos [2\pi\{(2f_x - p)\, x_i + (2f_y - q)\, y_i\}] \neq Na_{pq} \tag{2.13}$$

unless $2(f_x x_i + f_y y_i)$ is integer for all $i = 1, \ldots, N$. Thus whereas the lattice leads to a natural choice of Fourier frequencies, for marked point processes we have to choose an appropriate strategy for selecting a suitable frequency range. This problem is compounded by the fact that the scales of pattern for the coordinates $\{x_i, y_i\}$ may well be substantially different from those associated with the spatial mark structure $\{X_i\}$. For example, points might be controlled by a localized (i.e. high-frequency) inhibition process, whereas marks might be generated by a long-range (i.e. low-frequency) environmental effect, and it is clearly unrealistic to expect a single frequency range to cope with both given that we have only $N/2$ degrees of freedom available. In general it will therefore be necessary to study the spatial distributions of the points and the marks separately.

To perform specific tests of hypothesis, extending BRILLINGER's (1972) one-dimensional argument immediately shows that the two-dimensional point spectral estimates $\{\hat{f}(\underline{\omega})\}$ are, for large N, distributed as

$$2\hat{f}(\underline{\omega})/f(\underline{\omega}) \sim \chi^2_2 \qquad (\underline{\omega} \neq \underline{0}) \tag{2.14}$$

(see MUGGLESTONE and RENSHAW, 1996). Thus spectral tests for specific frequencies $\underline{\omega}$ are easily made by direct reference to χ^2-tables. Other test procedures (GREENWOOD/KIMBALL, KOLMOGOROV/SMIRNOV and ANDERSON/DARLING) are developed for purely point patterns in MUGGLESTONE and RENSHAW (2001), and it would be interesting to extend their application to marked point processes. However, the χ^2-test performed uniformly best in Mugglestone and Renshaw's point analyses, and it is sensible to retain it for our ubiquitous needs here. In virtually all fields of application the concept of *complete spatial randomness* (CSR) provides a useful benchmark against which we can assess observed pattern (DIGGLE, 1981). The associated 'null-distribution' is the two-dimensional homogeneous Poisson process (HPP), in which all points are distributed across the plane independently of one another (DIGGLE, 1983). Such independence means that the second-order intensity function $\gamma(\underline{a}, \underline{b}) \equiv 0$, whence (2.8) yields $f(\underline{\omega}) = f(\omega) = \lambda = N$ (since we are working within the unit square). Thus to detect departures from CSR we need to see whether the periodogram is 'flat'. Specifically, result (2.14) implies that

$$2\hat{f}(\underline{\omega})/N \sim \chi^2_2 \qquad (\underline{\omega} \neq \underline{0})\,. \tag{2.15}$$

Often we are interested in detecting the possible presence of specific scales of pattern or directional effects, and this is easily achieved by representing each spectral estimate $\hat{f}(\omega_p, \omega_q) = I_{pq}$ in the polar form $(\hat{f}_R(r), \hat{f}_\Theta(\theta))$, where $r = \sqrt{(p^2 + q^2)}$ and $\theta = \tan^{-1}(p/q)$ (see RENSHAW and FORD, 1983, 1984). Here $\hat{f}_R(r)$ is called the *R*-spectrum, and summarises average periodogram values for ordinates with similar values of r. Its prime use is to investigate scales of pattern under the assumption of isotropy. The Θ-spectrum, $\hat{f}_\Theta(\theta)$, summarises average periodogram values for ordinates with similar values of θ, and is used to investigate directional effects. We may write

$$\hat{f}_R(r) = (1/n_r) \sum_{p,q} I_{pq} \quad \text{and} \quad \hat{f}_\Theta(\theta) = (1/n_\theta) \sum_{p,q} I_{pq}\,, \tag{2.16}$$

where the summations are taken (for example) over all the n_r and n_θ periodogram ordinates (p, q) for which $r - 1 < \sqrt{(p^2 + q^2)} \leq r$ and $\theta - 5^\circ \leq \tan^{-1}(p/q) < \theta + 5^\circ$. Experience has shown this particular binning allocation to be a useful 'first try'. Note that I_{00} is excluded from this averaging procedure, as are I_{pq} for $p = 0$; $-f_x < q < 0$ and $q = f_y$; $0 \leq p \leq f_x$. The corresponding polar 'null-distributions' corresponding to (2.15) for testing against CSR are given by

$$\hat{f}_R(r)/N \sim (1/2n_r)\, \chi^2_{2n_r} \qquad (r = 1, 2, \ldots)\,, \tag{2.17}$$

$$\hat{f}_\Theta(\theta)/N \sim (1/2n_\theta)\, \chi^2_{2n_\theta} \qquad (\theta = 0^\circ, 10^\circ, \ldots, 170^\circ)\,. \tag{2.18}$$

The associated significance levels for each individual r and θ value then provide a measure of strength for patterns with that wavenumber and direction. Care must be taken not to interpret these measures too literally, since unlike lattice period-

ogram values the point and mark periodograms, I_{pq}^{P} and I_{pq}^{M}, may exhibit some degree of dependence.

Given that different test procedures emphasize different aspects of spatial pattern, pragmatism demands that we use all available techniques if we are to maximize information on spatial structure. Clearly, if the pattern generating mechanism is governed solely by nearest-neighbour distances, then nearest-neighbour and local correlation estimators will possess optimal properties. Conversely, if pattern is induced by an external wave agency then the spectral approach should perform best. In practice, generating mechanisms lie between these two extremes, but it is the fact that the correlation approach does not lend itself easily to coping with directional effects that makes the periodogram a natural first choice. In fairness, OHSER and STOYAN (1981) describe an anisotropic version of RIPLEY's (1976) K-function, namely $K(\theta, t)$, which relates to the expected number of further events with orientation θ, but despite its apparent usefulness it appears not to have been widely used. The key difference is that I_{pq}, $\hat{f}_R(r)$ and $\hat{f}_\Theta(\theta)$ are based on Fourier coefficients, and so involve *all* the data values, whilst $K(\theta, t)$ involves only those point-pairs whose orientation lies close to θ. So $\hat{f}_\Theta(\theta)$ is likely to be a more powerful detector of directional effects than $K(\theta, t)$; though it would be useful to undertake a comparative study between these two forms of estimator.

For many spatial processes determining the theoretical spectrum $f(\underline{\omega})$ is too difficult to be worthwhile undertaking, and using simulation to construct empirical spectra is often the preferred route (e.g. RENSHAW and FORD, 1984, for lattice spectra; MUGGLESTONE and RENSHAW, 1996, for point spectra). In some simple cases, however, exact derivation is possible. For example, in the modified Thomas cluster process 'parents' are distributed randomly in space with intensity λ, with each parent giving rise to a Poisson (μ) number of offspring, each of which is then independently and isotropically displaced by a Normal $(0, \sigma^2)$ radial distance (see THOMAS, 1949; NEYMAN and SCOTT, 1958 and also STOYAN, 1992). Here

$$f(\underline{\omega}) = \mu\lambda\{1 + \mu \exp(-\omega^2\sigma^2)\} \tag{2.19}$$

(BARTLETT, 1964) and

$$K(t) - \pi t^2 = (1/\lambda)\,[1 - \exp(-t^2/4\sigma^2)]\,, \tag{2.20}$$

and both have the same "$\exp(-z^2)$" structure, though there is no simple relation between them that is easy to interpret. A similar comparison arises from using Bartlett's suggested isotropic form

$$\gamma(t) = (\lambda v/2)\,(t^2/\sigma^2 - 2)\exp\{-t^2/2\sigma^2\} \tag{2.21}$$

for inhibition between plants; λ is the intensity of the inhibition process, and v and σ^2 reflect the strength and scale of inhibition, respectively. The spectrum

$$f(\underline{\omega}) \equiv f(\omega) = \lambda\{1 - v\sigma^2\omega^2 \exp(-\sigma^2\omega^2/2)\}\,, \tag{2.22}$$

and so $f(\omega)$ reaches a maximum at frequency $\omega = 1/\sigma$ which corresponds to wavelength $1/\omega = \sigma$. This is indicative of the same scale of pattern as given by the correlation analysis, since both $\gamma(r)$ and $K(r) - \pi r^2$ switch sign as r increases through σ. Both of these examples relate to point processes, and it would be worthwhile developing parallel results for marked point processes.

3. Perturbing Locations

3.1 *Perturbing lattice coordinates*

Consider a situation in which plants/trees are supposed to be planted on a lattice, but because of error in determining the intended lattice coordinates (s, t), the true coordinates are $(s + \epsilon_{st}/m, t + \eta_{st}/n)$, where $s = 1, \ldots, m$; $t = 1, \ldots, n$ and the perturbations $\{\epsilon_{st}, \eta_{st}\}$ are i.i.d. bivariate random variables with $E(\epsilon_{st}) = E(\eta_{st}) = 0$, $\mathrm{Var}\,(\epsilon_{st}) = \sigma_\epsilon^2$, $\mathrm{Var}\,(\eta_{st}) = \sigma_\eta^2$ and $\mathrm{Cov}\,(\epsilon_{st}, \eta_{st}) = \sigma_{\epsilon\eta}$. Then to assess how close the (now incorrect) lattice periodogram $\{I_{pq}^L\}$ lies to the (true) mark periodogram $\{I_{pq}^M\}$, we need to compare the lattice Fourier coefficients $\{A_{pq}, B_{pq}\}$ (2.9) to the corresponding mark Fourier coefficients

$$a_{pq} + ib_{pq} = \sum_{s=1}^{m} \sum_{t=1}^{n} (X_{st} - \bar{X}) \exp\left[2\pi i\{ p(s + \epsilon_{st}/m) + q(t + \eta_{st}/n)\}\right]. \tag{3.1}$$

Denote

$$\gamma_{pq} = p^2\sigma_\epsilon^2/m^2 + 2pq\sigma_{\epsilon\eta}/mn + q^2\sigma_\eta^2/n^2 \tag{3.2}$$

with $r^2 = (1/mn) \sum_{s=1}^{m} \sum_{t=1}^{n} (X_{st} - \bar{X})^2$. Then expanding a_{pq} and b_{pq} in powers of ϵ_{st} and η_{st} leads, after some algebraic manipulation, to

$$E[I_{pq}^M] \simeq I_{pq}^L + 4\pi^2\gamma_{pq}(r^2 - I_{pq}^L). \tag{3.3}$$

If, for example, $\{X_{st}\}$ is a white noise process, then $I_{pq}^L \simeq s^2$ for all p, q, so $E[I_{pq}^M] \simeq I_{pq}^L$ and the spectrum is essentially unchanged. Any discrepancies are magnified most at the (lattice) Nyquist frequency $(m/2, n/2)$, for which the factor $4\pi^2\gamma_{pq} = 4\pi^2(\sigma_\epsilon^2 + 2\sigma_{\epsilon\eta} + \sigma_\eta^2)$. This is to be expected, since points which move towards each other will cause a substantial change in the high-frequency components of $\{I_{pq}^M\}$ relative to the original $\{I_{pq}^L\}$. In contrast, if $\{X_{st}\}$ follows a pure cosine wave with frequency (p', q'), then $I_{p'q'}^L = Nr^2$ and $I_{pq}^L = 0$ otherwise. So now

$$E[I_{pq}^M] \simeq 4\pi^2\gamma_{pq}r^2 \quad \text{for} \quad (p, q) \neq (p', q'), \tag{3.4}$$

which increases with increasing (p, q); whilst for $(p, q) = (p', q')$

$$E[I_{p'q'}^M] \simeq Nr^2 + 4\pi^2\gamma_{p'q'}(r^2 - Nr^2) \simeq Nr^2(1 - 4\pi^2\gamma_{p'q'}), \tag{3.5}$$

which decreases as (p', q') increases. This assumes, of course, that σ_ϵ^2, σ_η^2 and $\sigma_{\epsilon\eta}$ are small enough to justify neglecting terms of order $o(\epsilon^2, \eta^2)$. Even so, (3.5) clearly places a restriction on γ_{pq} if our approximation is to remain valid since it gives $E[I^M_{p'q'}] < 0$ if $\gamma_{p'q'} > 1/4\pi^2$. For illustration, suppose we wish to restrict the change in $E[I^M_{pq}]$ to 10% where $m = n = 24$, $\sigma_\epsilon^2 = \sigma_\eta^2 = \sigma^2$ and $\sigma_{\epsilon\eta} = 0$. Then (3.5) yields

$$\gamma_{p'q'} = \sigma^2(p'^2 + q'^2)/24^2 < 1/(40\pi^2) \simeq 1/400\,, \quad \text{i.e.} \quad \sigma^2 < 1.44/(p'^2 + q'^2)\,.$$

Thus if:	$p' = q' = 1$	(single diagonal wave)	we need $\sigma < 0.85$;
	$p' = 3,\ q' = 4$	(medium-frequency wave)	we need $\sigma < 0.24$;
	$p' = q' = 12$	(Nyquist frequency)	we need $\sigma < 0.071$;
	$p' = q' = 24$	(double Nyquist frequency)	we need $\sigma < 0.035$.

Clearly, the larger the frequency component (p', q'), the smaller is the allowable perturbation. Indeed, at the Nyquist frequency we have $2\sigma/m < 0.006$, so only very small displacements are allowed before the lattice and marked point spectra produce substantially different results.

This scenario of a displaced lattice provides an excellent illustration of the type of situation for which spectral techniques will considerably outperform nearest-neighbour methods. For example, MUGGLESTONE and RENSHAW (1996) disturb the locations of a 10×10 lattice by $N(0, 0.02^2)$, and although the spatial point pattern shows evidence of a minimum inter-event distance the underlying lattice structure is impossible to detect by eye. However, the (point) periodogram has two very large components at $p = 0$, $q = 10$ and $p = 10$, $q = 0$, thereby providing strong evidence for the existence of an underlying lattice structure.

3.2 *The covering lattice*

In the converse situation the exact locations of a m.p.p. are replaced by the nearest grid points of a covering lattice. This would arise if we wished to: (i) allow direct use of the lattice autocovariance and periodogram estimators, (1.5) and (1.6); or, (ii) assess the effect of recording point locations to a given number (d) of decimal places. In case (ii) I^L_{pq} and I^M_{pq} are clearly equivalent when the former is evaluated over a $10^d \times 10^d$ lattice. Note that there is an implicit difficulty here. For the mark process has a fixed number of associated degrees of freedom, whereas the covering lattice of zeros and marks can have an unlimited number since the lattice can be arbitrarily fine and a zero is deemed to carry the same information content as a mark.

We therefore now observe marks at their locations $\{(s + \epsilon_{st},\ t + \eta_{st})\}$ and compare the resulting periodogram with that derived via the approximating covering lattice $\{(s, t)\}$. In terms of the cosine wave with frequency (p', q'), this means that the Fourier coefficients are given by

$$a_{pq} = \sum_{s=1}^{m} \sum_{t=1}^{n} \cos\left[2\pi\left(p'(s + \epsilon_{st})/m + q'(t + \eta_{st})/n\right)\right] \times \cos\left[2\pi\left(p(s + \epsilon_{st})/m + q(t + \eta_{st})/n\right)\right] \tag{3.6}$$

with a similar expression for b_{pq}. Expanding the cosine terms to $O(\epsilon^2, \eta^2)$, as before, then shows that for (p', q') not an integer multiple of $(m/2, n/2)$, we have: for $(p, q) \neq (p', q')$

$$E[I^M_{pq}] \simeq \pi^2(\gamma_{p'+p,q'+q} + \gamma_{p'-p,q'-q}) = 2\pi^2[(p'^2 + p^2)\,\sigma^2_\epsilon/m^2 + 2(p'q' + pq)\,\sigma_{\epsilon\eta}/mn + (q'^2 + q^2)\,\sigma^2_\eta/n^2]; \tag{3.7}$$

whilst for $(p, q) = (p', q')$

$$E[I^M_{p'q'}] \simeq (mn/4) + 4\pi^2\gamma_{p'q'} = (mn/4) + 4\pi^2[p'^2\sigma^2_\epsilon/m^2 + 2p'q'\sigma_{\epsilon\eta}/mn + q'^2\sigma^2_\eta/n^2]. \tag{3.8}$$

Note that the background 'spectral clutter' (3.7) increases as $(p, q)^2$.

Since the variance of a pure cosine wave is 1/2, it follows that for the corresponding lattice spectrum $I^L_{p'q'} = I^L_{m-p',n-q'} = mn/4$. Comparison with the marked spectral result (3.8) suggests that whilst $I^M_{p'q'}$ will still lie near to $mn/4$, $I^M_{m-p',n-q'}$ might be substantially different. Indeed, it is easily shown that

$$a_{m-p,n-q} = a^c_{pq} + b^s_{pq} \quad \text{and} \quad b_{m-p,n-q} = a^s_{pq} - b^c_{pq}, \tag{3.9}$$

where $\{a^c_{pq}, b^c_{pq}\}$ and $\{a^s_{pq}, b^s_{pq}\}$ denote the Fourier coefficients of the modified processes $\{X(s+\epsilon_{st}, t+\eta_{st}) \cos[2\pi(\epsilon_{st} + \eta_{st})]\}$ and $\{X(s + \epsilon_{st}, t + \eta_{st}) \sin[2\pi(\epsilon_{st} + \eta_{st})]\}$, respectively. Clearly, if $\epsilon_{st}, \eta_{st} \equiv 0$ then $(a_{m-p,n-q}, b_{m-p,n-q}) \equiv (a^c_{pq}, -b^c_{pq}) \equiv (a_{pq}, -b_{pq})$ since $(a^s_{pq}, b^s_{pq}) \equiv 0$, whence $I^M_{m-p,n-q} \equiv I^M_{pq}$. However, as Var (ϵ_{st}) and Var (η_{st}) increase, the multiplicative cosine and sine factors swiftly take hold and $I^M_{m-p,n-q}$ rapidly departs from I^M_{pq}. Indeed, this departure accelerates with increasing frequency. To illustrate this effect we sampled the cosine wave $X_{st} = \cos[2\pi(3s + 4t)/24]$ at locations generated by a 24×24 lattice perturbed by the random uniform displacements $kU(-0.5, 0.5)$. Thus if $k = 1$ then neighbouring points can just touch; if $k > 1$ then they can cross over; whilst if $k = 24$ the perturbation fills the entire square, i.e. the original lattice structure is destroyed. Simulation yielded the following results:

k	maximum perturbation	$I^M_{3,4}$	$I^M_{21,20}$	reduction in $I^M_{21,20}$
0	nil	144	144	nil
0.01	tiny	144.2	143.6	slight
0.1	small	145.0	132.2	nearly 10%
0.2	still small	143.3	116.4	substantial
0.5	half inter-lattice point distance	141.5	25.9	over 80%
1.0	inter-lattice point distance	143.1	0.5	completely obliterated

Thus whilst $I^M_{3,4}$ hardly deviates from the lattice value $I^L_{3,4} = 144$, the high-frequency component $I^M_{21,20}$ swiftly decays to zero as k approaches one.

4. Analysis of Simulated Marked Point Patterns

Not only are exact theoretical spectral results, such as (2.19) for a cluster process and (2.22) for an inhibition process quite rare, but even these just relate to pure point patterns (a few renewal examples are listed in COX and ISHAM, 1980 and CHANDLER, 1995). The development of theoretical spectral results for marked point processes is clearly a challenging problem for the future, and our current study of marked point spectra therefore proceeds via numerical examples. Their structure is kept deliberately simple in order to highlight the effects of periodicity, inhomogeneity, anisotropy, inhibition-versus-aggregation and mark/point interaction. Analysis of a specific forestry data set is undertaken in Section 5.

Example 1: Cosine Wave/HPP: Figure 1a shows 400 points uniformly distributed in the unit square with marks

$$m_i = 2 + \cos\left[2\pi(px_i + qy_i)\right] + k(U - 1/2) \qquad (i = 1, \ldots, 400)\,, \qquad (4.1)$$

where $p = 4$, $q = 3$, $k = 2$ and $U \sim U(0,1)$. The corresponding point spectrum (Figure 1b) has $\max\,(I^P_{pq}) = 5.1159$ at $p = 8$, $q = 3$, whence applying Fisher's test (PRIESTLEY, 1981) to $g = \max\,(I^P_{pq}) / \sum I^P_{pq} = 0.0274$ gives $\Pr\,(g > 0.0274) \simeq 0.56$ which is clearly not significant (as expected under CSR). To examine the point polar spectrum (2.16) we first scale $\hat{f}_R(r)$ and $\hat{f}_\Theta(\theta)$ to sum to 100%. Then under CSR each $H_{pq} = I_{pq} / \sum I_{pq}$ has $E[H_{pq}] = 1/N'$, so given (2.15) we have $H_{pq} \sim (1/2N')\,\chi^2_2$; here $N' = 201 \simeq N/2 = 200$ is the number of periodogram values used. Thus in terms of the scaled polar spectrum $\{R_r, \Theta_\theta\}$, we have $E(R_r) = 100(n_r/N')$ giving $R_r \sim 100(n_r/N')\,(1/2n_r)\,\chi^2_{2n_r}$, i.e.

$$(2N'/100)\,R_r \sim \chi^2_{2n_r} \qquad (r = 1, 2, \ldots)$$

with

$$(2N'/100)\,\Theta_\theta \sim \chi^2_{2n_\theta} \qquad (\theta = 0^\circ, 10^\circ, \ldots)\,. \qquad (4.2)$$

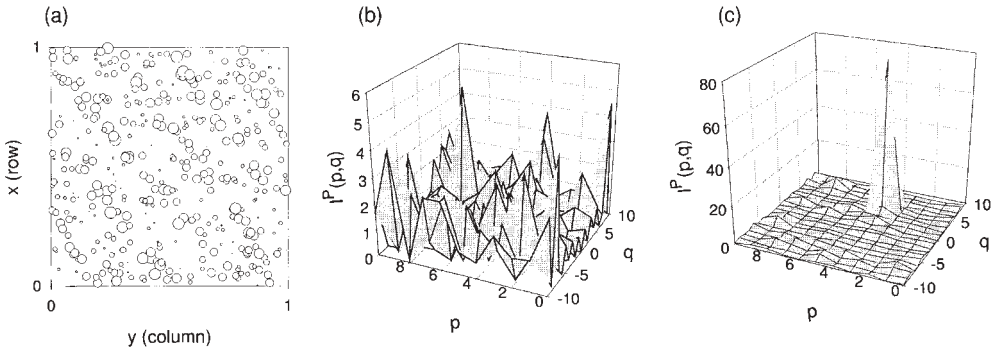

Fig. 1. (a) 400 uniformly distributed points with noisy cosine marks (4.1) (radii proportional to mark); (b) point periodogram; (c) mark periodogram

Although these results do not hold exactly, since the I_{pq} are not totally independent, they do provide perfectly acceptable *measures* of spatial structure. As anticipated, none of the R_r and Θ_θ values produce significant results. The marked spectrum (Figure 1c) shows a clear maximum at frequency $(4, 3)$, with $I^M_{43} = 98.2$ for $k = 0$, 99.9 for $k = 0.5$ and 105.0 for $k = 2.0$; at all other frequencies $I^M_{pq} \leq 2.7$, 2.7 and 6.2, respectively. Thus the spectral signature of the underlying cosine wave is effectively unchanged even when the wave is submerged by high noise levels. The effect of increasing k on the polar R- and Θ-spectra is minimal.

Example 2: Cosine Wave/IHPP: To examine the effect of adding spatial point structure (Figure 2a) the 400 points were then distributed according to an inhomogeneous Poisson process (IHPP) with intensity $\lambda(x, y) \equiv \lambda(y) = 2 + \sin(4\pi y)$, i.e. frequency 2 across the columns. Thus points are accepted only if $U \leq \lambda(y)/3$ where $U \sim U(0, 1)$; so points generated at $y = 1/8, 5/8$ are always kept, but those at $y = 3/8, 7/8$ are only retained with probability 1/3. The point spectrum (Figure 2b) yields $I^P_{02} = 30.43$ with $I^P_{pq} \leq 4.56$ otherwise, thereby providing extremely strong evidence in support of the underlying point wave structure. Although the mark spectral maximum is virtually unchanged at $I^M_{43} = 102.69$, there are now two spurious secondary peaks (Figure 2c) $I^M_{41} = 10.42$ and $I^M_{45} = 9.36$ ($I^M_{pq} \leq 3.40$ elsewhere). These correspond to mark/point interactions forming 'anomalous' waves at frequencies $(4,3) \pm (0,2)$, and highlight the danger of jumping to conclusions about secondary spectral peaks too readily. All three spectral peaks are robust with respect to large values of added $k(U - 1/2)$ noise.

Progress in understanding such mark/point interaction can be made by considering the *cross*-periodogram

$$I^{(\text{cross})}_{pq} = (a_{pq}c_{pq} + b_{pq}d_{pq})/N\,. \tag{4.3}$$

Here $\{a_{pq}, b_{pq}\}$ denote the mark Fourier coefficients (2.11), and $\{c_{pq}, d_{pq}\}$ the point Fourier coefficients

$$c_{pq} = \sum_{i=1}^{N} \cos\left[2\pi(px_i + qy_i)\right] \quad \text{and} \quad d_{pq} = \sum_{i=1}^{N} \sin\left[2\pi(px_i + qy_i)\right]. \tag{4.4}$$

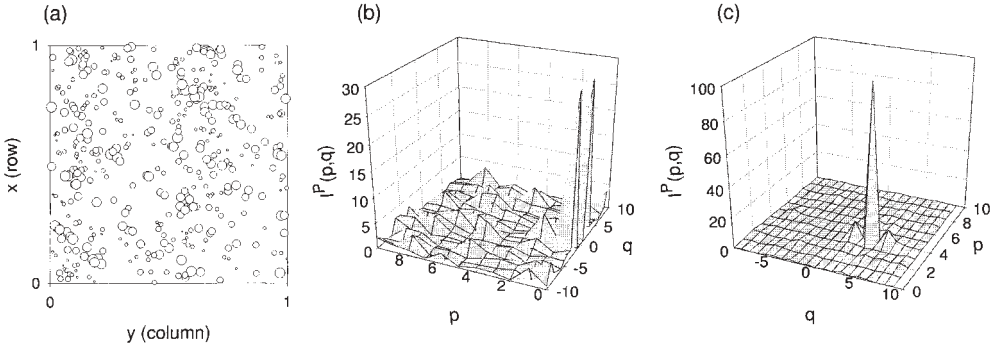

Fig. 2. As Figure 1, but with inhomogeneous point intensity $\lambda(x, y) = 2 + \sin(4\pi y)$

Since the function (4.3) sits 'midway' between $I^M_{pq} = (a^2_{pq} + b^2_{pq})/N$ and $I^P_{pq} = (c^2_{pq} + d^2_{pq})/N$, it might well provide an appropriate measure of mark/point interaction. The rationale is that on denoting the *raw mark* Fourier coefficients by

$$\alpha_{pq} = \sum_{i=1}^{N} X_i \cos\left[2\pi(px_i + qy_i)\right] \quad \text{and} \quad \beta_{pq} = \sum_{i=1}^{N} X_i \sin\left[2\pi(px_i + qy_i)\right], \tag{4.5}$$

we have

$$I^{(\text{raw mark})}_{pq} \equiv (\alpha^2_{pq} + \beta^2_{pq})/N = I^M_{pq} + \overline{X}^2 I^P_{pq} + 2\overline{X} I^{(\text{cross})}_{pq}. \tag{4.6}$$

So if there is no cross-spectral component then the mark and point periodograms are effectively additive.

As the cosine mark structure in Examples 1 and 2 is global in nature, we also consider three local mark interaction scenarios under HPP, namely:

(i) independent uniform: $X_i = 1 + U(-0.5, 0.5)$ (Figure 3a);

(ii) inhibition: $X_i = \begin{cases} 1 & \text{if } |x_i - x_j| < 0.03 \text{ for all } j \neq i \\ 2 & \text{if not} \end{cases}$ (Figure 3b);

(iii) mutual enhancement: $X_i = \#$ points with $|x_i - x_j| < 0.04$ for all $j \neq i$ (Figure 3c).

Analysis of the marked polar spectra yields the following significance probabilities. Under (i) we have 0.208 for R_{11} and 0.069 for Θ_{160}, neither of which provides evidence of spatial structure (as expected). Whilst (ii) gives 0.033 for R_4 and 0.066 for Θ_{130}; so there is evidence at the 5% level of a scale of pattern at distance $\simeq 0.25$, though there is no evidence of any directional structure. Finally, (iii) yields 0.010 for R_6 and 0.065 for Θ_{170}; the scale 1/6 implies about 36 separate clusters, which seems visually plausible. Again, there is no evidence for directional effects. However, although this exercise shows that spectral analysis can reveal mark structure superimposed on random locations, we still need to determine whether it is effective when the points themselves possess spatial structure.

Example 3: Inhibited Points: Consider a hard-core sequential inhibition process in which no new point (x', y') is allowed inside the ellipse $(x - x')^2 + 4(y - y')^2 \leq 0.058^2$ centred on the old points (x, y); the value 0.058^2 ensures (almost) maximum packing. Given that this is a pure nearest-neighbour structure, it clearly presents a hard test for the spectral approach. Now at $x = x'$, $|y' - y| \leq 0.029$, and at $y = y'$, $|x' - x| \leq 0.058$; so the maximum (point) frequencies are $f_y = 1/0.029 = 34.48$ and $f_x = 1/0.058 = 17.24$. Using the frequency range $0 \leq p, q \leq 20$ yields significance probabilities

$$p^{(r)} < 0.005 \qquad (18 \leq r \leq 25)$$

and

$$p^{(\theta)} < 0.05 \qquad (45^\circ < \theta < 85^\circ;\ 95^\circ < \theta < 125^\circ).$$

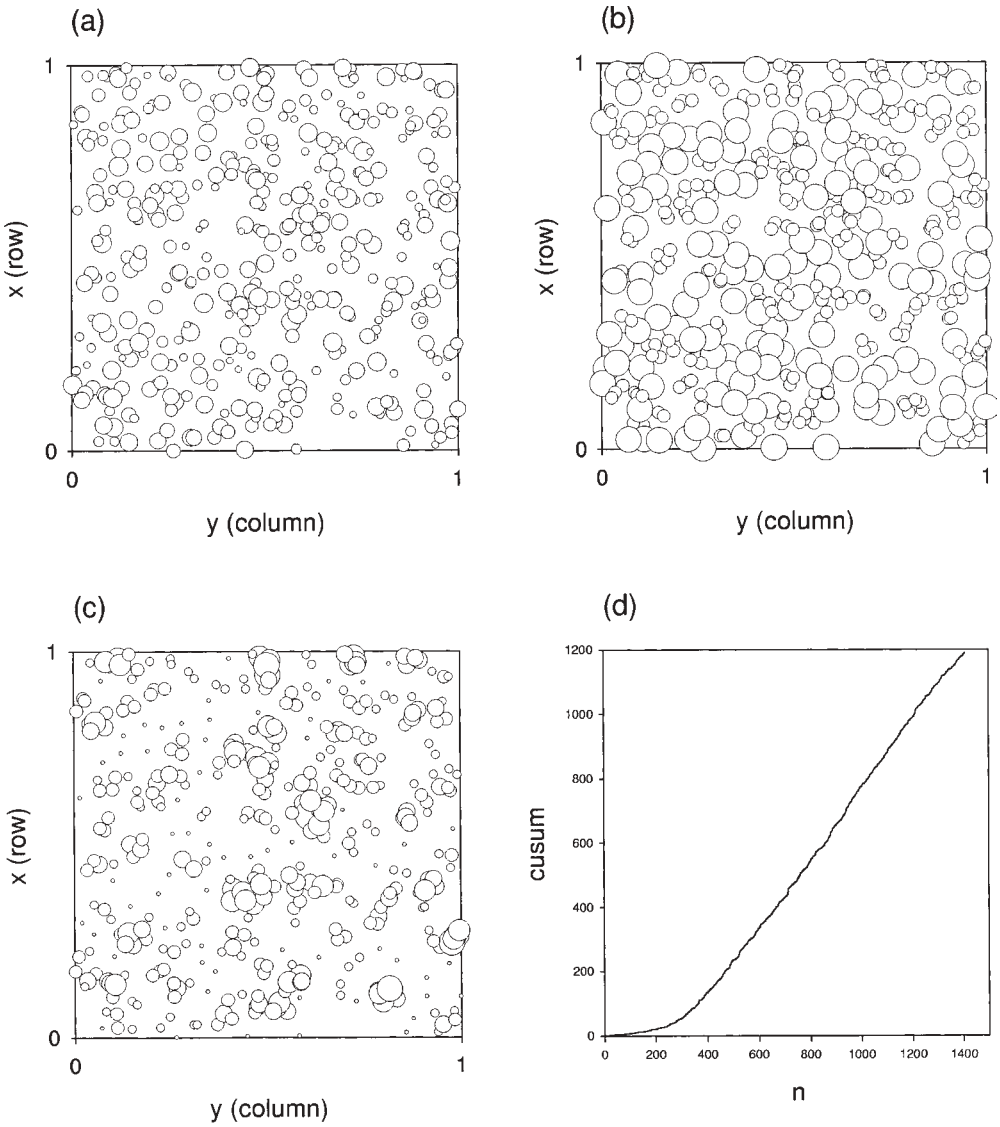

Fig. 3. 400 uniformly distributed points with three local interaction mark regimes: (a) independent uniform, (b) inhibition and (c) mutual enhancement (radii proportional to $3 \times$ mark, $3 \times$ mark and mark, respectively); (d) cusum point periodogram for a hard-core sequential elliptical inhibition process

The lower bound $r = 18$ is clearly in line with $f_x = 17.24$; though as $f_y = 34.48$ lies well beyond our frequency range $p, q = 1, \ldots, 20$ we cannot expect to detect it. Extending this range may cause serious degredation of the analysis since there would be far more periodogram values than data points. The directional effects shown in the Θ-spectrum highlight the diagonal lineations of the ellipse centres under maximum packing.

Note that the polar spectra can also be expressed in terms of cusums. For example, with a 30×30 frequency grid first sort the $r = \sqrt{(p^2 + q^2)}$-values into ascending order, thereby reordering the $\{I_{pq}\}$ into $\{I_{pq}^{(n)}\}$ over $n = 1, \ldots 1801$ (excluding $p = 0$, $q = 0, \ldots 9$); all components for which $r > 30$ are deleted to ensure that all directions are equally represented. A cusum plot (Figure 3d) shows that $I_{pq}^{(n)}$ increases relatively slowly until $n \simeq 420$, i.e. $r \simeq 16.3$, whereafter it rises at constant rate. Thus the switch-frequency $f_x = 17.24$ is clearly identified. Specific tests for the ordered $I_{pq}^{(n)}$-values could be made by grouping them into batches of size s, and calculating the associated significance probability based on χ^2_{2s}. The Θ-spectrum could be considered similarly by ordering with respect to increasing values of θ.

Example 4: Superimposed Marks: The above three mark regimes, with disc radii of 0.038 (inhibition) and 0.05 (enhancement), were then superimposed on this elliptically inhibited point pattern. (i) Uniform: the strong spatial point structure appears to exert no influence on the mark spectrum. (ii) Inhibition: there are strong effects at low and middle frequencies which provide an indicator of clump size; almost all the clumps are distinct, and this is reflected by the lack of significance at $r = 1$. Moreover, interaction between the point and mark structures is clearly visible in the Θ-spectrum. Indeed, not only does the lowest $p^{(\theta)}$-value of 0.00073 at $\theta = 80^\circ$ confirm the inherent lack of (point) isotropy, but the successively *high* significance probabilities 0.97 ($\theta = 0^\circ$), 0.995 ($\theta = 10^\circ$), 0.998 ($\theta = 20^\circ$), 0.9997 ($\theta = 160^\circ$) and 0.86 ($\theta = 170^\circ$) provide a major pointer to the *absence* of spatial structure in the band $-25^\circ \leq \theta \leq 25^\circ$. (iii) Attraction: here the R-spectrum is concentrated in the lower frequencies with a sharp cut-off between $r = 5$ ($p^{(r)} = 0.0044$) and $r = 6$ ($p^{(r)} = 0.79$). This compares with $r = 10$ and 11 under the inhibition structure (ii). Moreover, there is now a significant component at $r = 1$, and this is in accordance with large marks forming a 'clique' right across the region. Another major contrast with (ii) is the lack of any directional component.

These simulated examples have been chosen to highlight specific issues and contrasts, and many other experiments could be performed (e.g. superimposing marks on point clusters). The fundamental point is that in any given spatial scenario it is either difficult or impossible to prejudge what the likely spectral outcome will be, and simulation experiments provide a powerful means of disentangling the individual point, mark and mark/point components of the underlying spatial process.

5. Analysis of Marked-Point Longleaf Pine Data

Such simulated analyses indicate the type of spectral structure likely to be encountered under independence, orientation, inhibition and aggregation. As such they provide useful touchstones when we explore real data sets, since the structure of both the point and mark estimators should provide good insight into the underlying pattern generating mechanism. To conclude, we shall therefore analyze a data set that has previously been extensively studied using a variety of space-domain approaches.

The longleaf pine data are from the Wade Tract, an old-growth forest in Thomas County, Georgia, and were collected by W. J. Platt and S. L. Rathbun with the support of the Tall Timbers Research Station, Tallahassee, Florida. These data (listed in Table 8.1, pp. 581–585, of CRESSIE, 1993) consist of the coordinates and diameters (at breast height) of all longleaf pine trees at least 2 cm in diameter at breast height (dbh, in centimetres) in 4 ha of forest in 1979. The x and y coordinates are distances (in metres) from the tree to the southern and eastern boundary, respectively. The data are mapped in his Figure 8.1 (p. 580) and are reproduced here in Figure 4. Note that this figure shows the locations as $(1 - x/200,\ 1 - y/200)$ in order to retain Cressie's

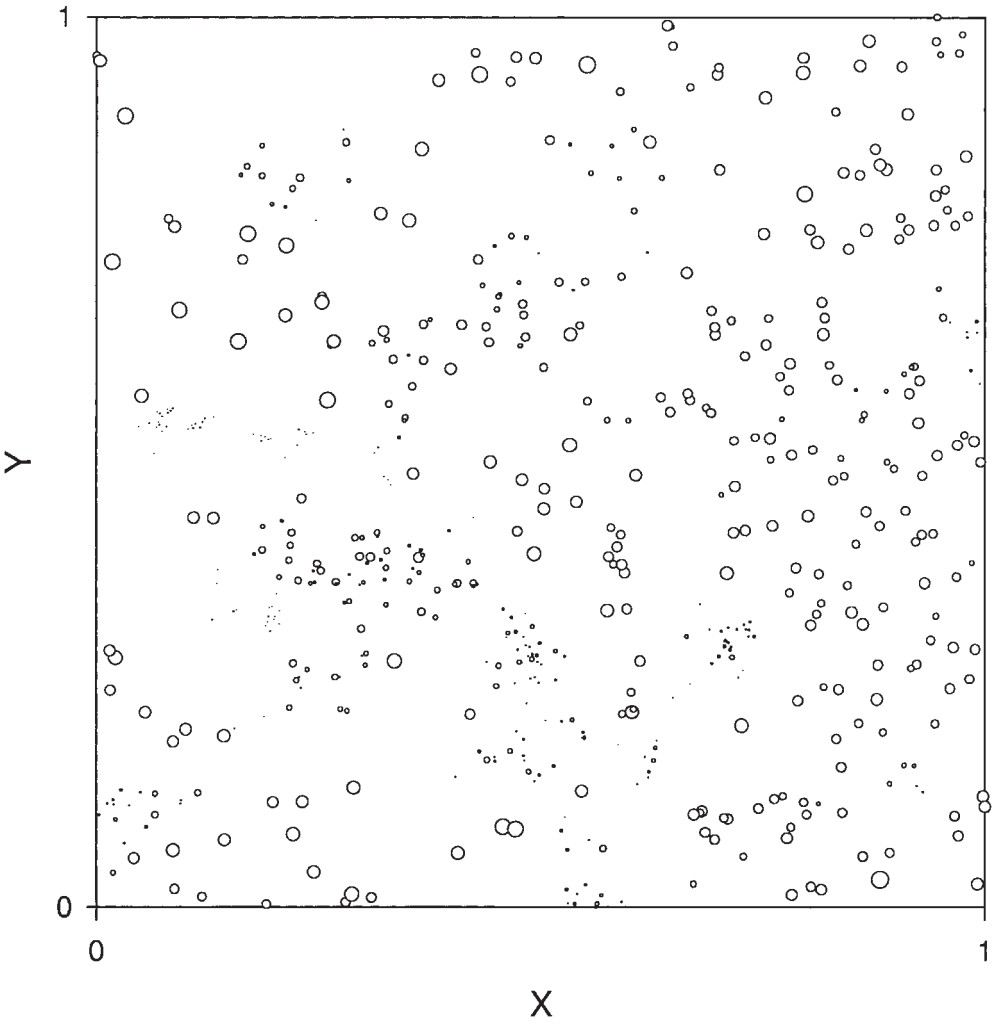

Fig. 4. Map of locations and relative diameters at breast height (dbh in centimetres) of 584 longleaf pines in the 200×200 (4-ha) study region of the Wade Tract in 1979. Locations show $(1 - x/200,\ 1 - y/200)$ of the coordinates given in Table 8.1 of Cressie (1993); bubble radius = dbh/20

top right to bottom left orientation and to ensure that coordinates lie in the unit square; the bubbleplot radii are $0.05 \times$ mark. On occasion, he refers to this sample area as the 'central study region' (4 ha), in order to differentiate it from the 'extended study region' which comprises the surrounding 12 ha border. Some of the material presented in Section 8.2 of CRESSIE (1993) can be found in RATHBUN and CRESSIE (1990). As CRESSIE (1993) notes, prior to European settlement, forests dominated by longleaf pine *(Pinus palustris)* occurred throughout most of the southern Atlantic and Gulf coastal plains of the United States. The Wade Tract is one of the largest remaining stands and is relatively free of disturbances by humans. There is evidence that this forest was present prior to European settlement. Longleaf pine is a fire-adapted species; ground fires occur frequently in these forests, removing most competing hardwoods. In addition to longleaf pine, there are a number of other tree species, predominantly the scrub oak species *Quercus incana*, *Quercus laevis*, *Quercus marilandica* and *Quercus margaretta*. These species are few in number and small in stature, and in the present study only the data for longleaf pines are considered. The 4 ha study region of the Wade Tract was chosen for its relatively gentle topography, for its absence of notable recent disturbances, and because all sizes of trees are represented; a random sample of 400 tree cores revealed all ages of trees up to 250 years. For more details see PLATT, EVANS, and RATHBUN (1988).

We first present a brief summary of CRESSIE's (1993) extensive space-domain analyses so that comparison can be made with the spectral approach. His Figure 8.3 depicts the locations of 100 non-overlapping circular quadrats, 6 m in radius, in the extended study region (16 ha). Pearson's χ^2-test on the frequency distribution of trees per quadrat indicates significant departure from spatial randomness; there are more empty quadrats and quadrats with five or more trees than would be expected under a Poisson distribution, and so trees appeared to be clustered. Blocking the trees into a 32×32 grid of 6.25×6.25 quadrats enables the analysis of contiguous quadrat data – a plot (his Figure 8.6) of mean square against block size is compared with a 95% simulation envelope obtained from 200 random rearrangements of the original quadrat counts. For large block sizes, mean squares lie above the upper acceptance envelope, indicating patches of size 50 m and 100 m square. Moreover, paired-quadrat variances (estimated from all possible pairs of quadrats) against distance between quadrat centres, suggests that variation between adjacent quadrats is smaller than would be expected for randomly arranged quadrat counts. This implies that there is some small-scale spatial homogeneity in quadrat counts. Use of a kernel density estimator based on a bandwidth of 40 m suggests that the point pattern is nonstationary; there is a clear trend of increasing intensity from the eastern to the western half of the study region. Peak intensities of more than $0.025\ \mathrm{m}^{-2}$ are found in a band extending from the west-central to the north-central part of the study region and in the northwestern corner. Intensities in the eastern portion are generally less than $0.015\ \mathrm{m}^{-2}$. Although a 40 m kernel is too large to show the fine structure of the spatial pattern evident in Figure 4 (several small clusters of densely packed small trees are

present), use of a smaller kernel size would result in smaller bias only at the expense of a large increase in variance. He presents results of 17 nearest-neighbour methods, both with and without edge correction, based on 10% sampling (his Table 8.7), which highlight the degree of clustering, together with parallel analyses using all 584 pines and 584 random points, and a discussion of the K-function approach.

Though CRESSIE (1993) does not provide a corresponding marked analysis, it would be possible to follow CRESSIE (1993, p. 717) and regard the tree coordinates as the locations of an irregularly spaced lattice, so that marks may be considered as spatial-lattice data and modelled accordingly (see, for example, his Chapter 6). Indeed, since marks and points are generated in a wholly integrated way, e.g. young trees in the shadow of large mature trees are more likely to die than those developing in the open, a 'true' analysis of marked point data should involve a simultaneous treatment of marks and points. Whilst there is a considerable literature available for point analysis and mark analysis conditional on point positions, there is relatively little on mark-point procedures. Even if there were, there would still be inferential difficulties since the underlying hypotheses would have to reflect assumptions on the process generating mechanisms.

Cressie observes that a Poisson cluster process (of offspring from parents) does not provide a very good fit to the data, and suggests that these models fail to fit the data because they ignore the dynamics of the biological processes that generated the spatial point pattern. He states that a proper analysis of these data would involve dynamic modelling of the birth process, the death process, and the growth process, with a view towards integrating these components back into a global model (e.g. RATHBUN and CRESSIE, 1990). RENSHAW and SÄRKKÄ (2001) pursue this route by allowing points to follow an immigration-death process, with random locations in the unit square taking uniformly distributed marks. These marks then develop according to a deterministic logistic growth process; points with negative marks are immediately deleted. They restrict themselves to Strauss-type pairwise interaction processes, and not only highlight the way in which Gibbs models are able to capture the interaction structure of the generating process, but also demonstrate that very few statistical indicators are needed to determine the essence of the process. This contrasts markedly with the relatively large number of estimators usually needed to characterise a process in terms of spectral, autocorrelation or K-function representations. Moreover, the Strauss-type procedure is robust, i.e. it is not crucial to know the exact process-generating mechanism. Whilst here the aim is to determine purely spatial, i.e. 'snapshot', summary measures from which we can infer underlying generating mechanisms of space-time stochastic processes, work is currently being undertaken to determine the extent to which spatial-temporal data can be analysed. The associated development of space-time spectral and autocorrelation techniques would enable an extremely useful comparison to be made with space-time Gibbs-type descriptors.

5.1 *Spectral point analysis*

Evaluating the point Fourier coefficients (4.4) over the $N = 584$ points (x_i, y_i) leads to the point spectrum $I^P_{pq} = (c^2_{pq} + d^2_{pq})/N$, shown in Figure 5a for

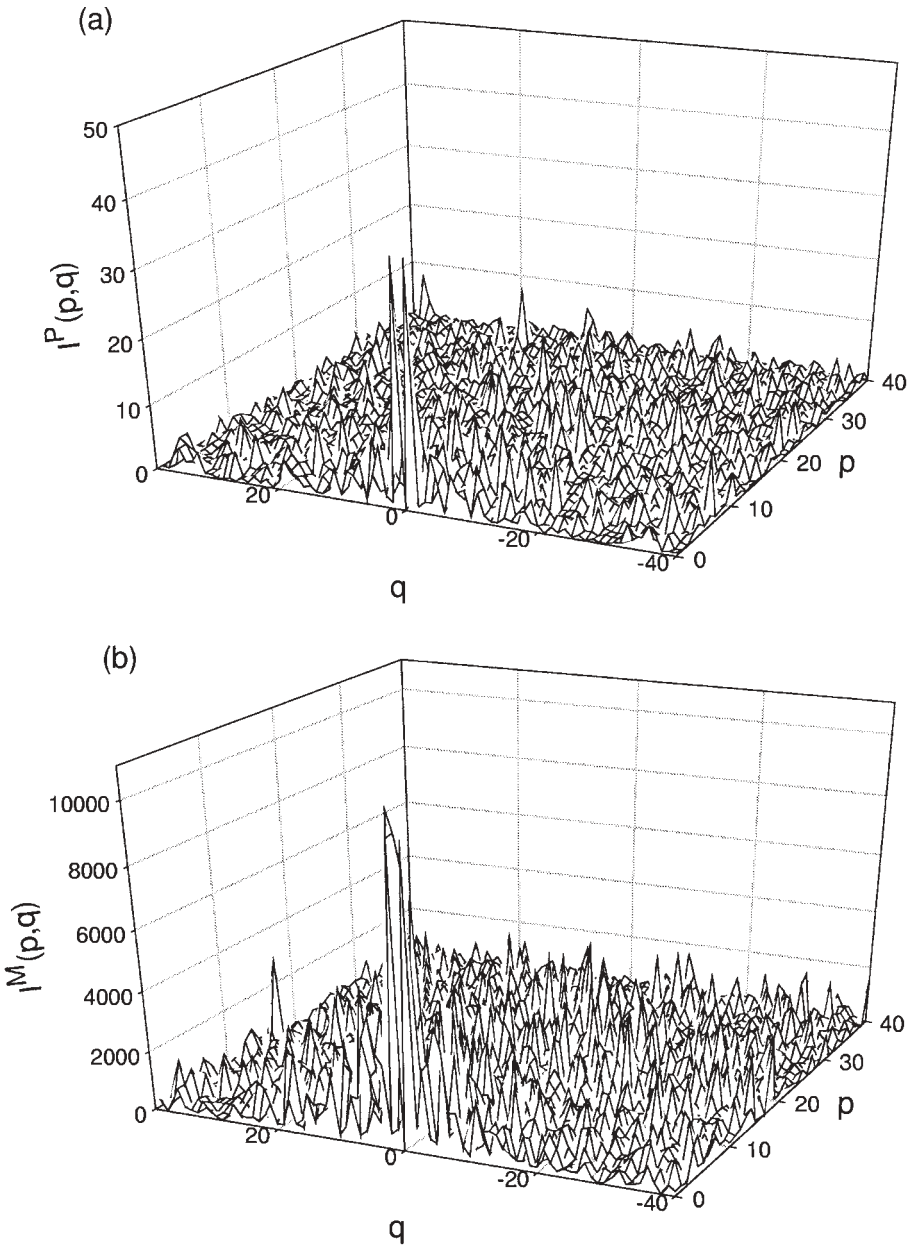

Fig. 5. (a) Point periodogram $\{I^P_{pq}\}$ and (b) mark periodogram $\{I^M_{pq}\}$ of the longleaf pine data, evaluated over $p = 0, \ldots, 40$; $q = -40, \ldots, 39$

$p = 0, \ldots, 40$; $q = -40, \ldots, 39$. Whilst this portrays no visually apparent structure (apart from 2 large peaks at $p = 0$, $q = \pm 1$ associated with slight spatial trend), the corresponding polar spectra are highly informative. Figures 6a and 6d show the corresponding R- and Θ-spectra expressed as a percentage contribution to the overall spectrum; output is binned into the intervals $[r, r+1)$ for $r = \sqrt{(p^2 + q^2)} = 1, 2, \ldots, 40$ and $[\theta - 5^\circ, \theta + 5^\circ)$ for $\theta = \tan^{-1}(p/q) = 0^\circ, 10^\circ, \ldots, 170^\circ$, taken over the rectangular frequency array $p = 0, \ldots, 40$; $q = -40, \ldots, 39$ minus the first and last sub-rows $p = 0$; $q = -39, \ldots, 0$ and $p = 40$; $q = -39, \ldots, -1$ (to ensure compatibility with the form for lattice periodograms). Note that we restrict $r \leq 40$ since higher frequencies relate to increasingly diagonal directions. To investigate the associated significance levels, let R_r and Θ_θ respectively contain n_r and n_θ elements, and denote $n_{\text{tot}} = \sum n_r = \sum n_\theta$. Then on paralleling (4.2) we have

$$(n_{\text{tot}}/50)\, R_r \sim \chi^2_{2n_r} \qquad (r = 1, 2, \ldots)$$

and

$$(n_{\text{tot}}/50)\, \Theta_\theta \sim \chi^2_{2n_\theta} \qquad (\theta = 0^\circ, 10^\circ, \ldots, 170^\circ)\,. \tag{5.1}$$

Figures 6b and 6c show the resulting percentage significance probabilities for the R-spectrum, and highlight that low R-values for $r \leq 12$ are strongly significant, being highly indicative of clustering since the spectrum is dominated by the relatively large inter-cluster distances. Since a frequency of 12 corresponds to a wavelength of $200/12 \simeq 17$ along the rows and columns, and $200\sqrt{2}/12 \simeq 24$ along the diagonals, this feature is suggestive of intercluster distances of the order of around 20 m and larger. This inference is not only in accord with the visual impression given by Figure 4, but is also in broad agreement with CRESSIE's (1993, p. 595) nested block quadrat value of 25×25 m.

Given that the lack of underlying orthogonality means that the I_{pq} are not fully independent of each other, we need to verify that these χ^2 measures are sufficiently robust to yield sensible significance values. Adopting a Monte Carlo approach, we therefore generated 99 sets of random point patterns each comprising 584 points, and performed the periodogram and polar analysis for each as above. Not only does superimposing the resulting R-spectral envelope on Figure 6a confirm that R-values are significant at the $\leq 1\%$ probability level, but evaluating the relative rank of the pine R-values and then plotting 100-rank against r (Figure 6b) shows almost perfect agreement with the χ^2 probability values. This strongly supports the use of the χ^2 statistic even though the assumptions on which it is based do not fully hold true.

Figures 6d, 6e and 6f show the parallel Θ-analyses, and highlight the existence of a row effect ($\theta \simeq 0^\circ$), together with a possible column effect ($\theta \simeq 90^o$). The former most likely relates to the nonstationary nature of the point pattern (mentioned earlier), namely a clear trend of increasing intensity from the eastern to the western half of the study region. The advantage of the spectral approach is that it

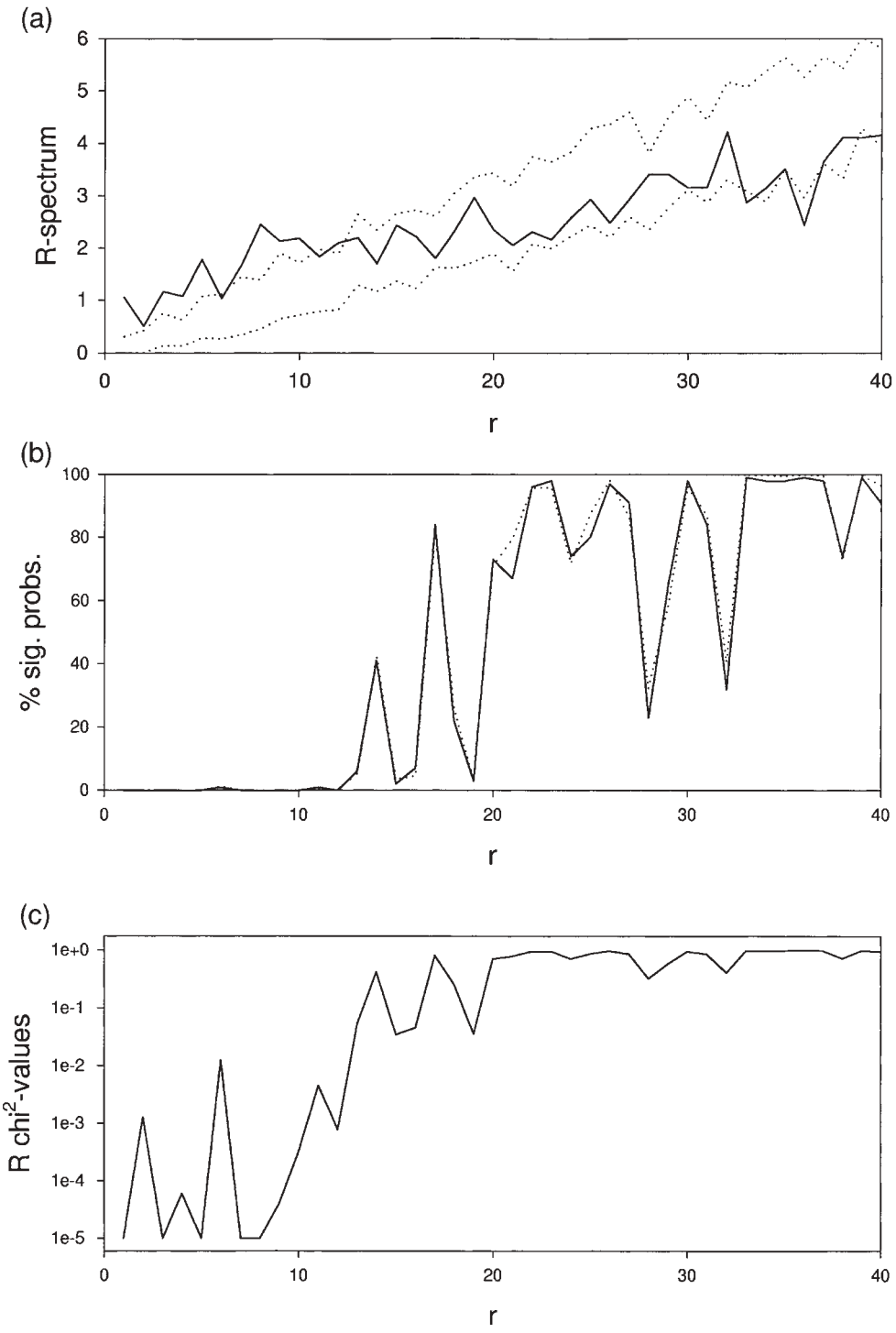
(a)
R-spectrum
0
1
2
3
4
5
6
0
10
20
30
40
r
(b)
% sig. probs.
0
20
40
60
80
100
0
10
20
30
40
r
(c)
R chi²-values
1e+0
1e-1
1e-2
1e-3
1e-4
1e-5
0
10
20
30
40
r

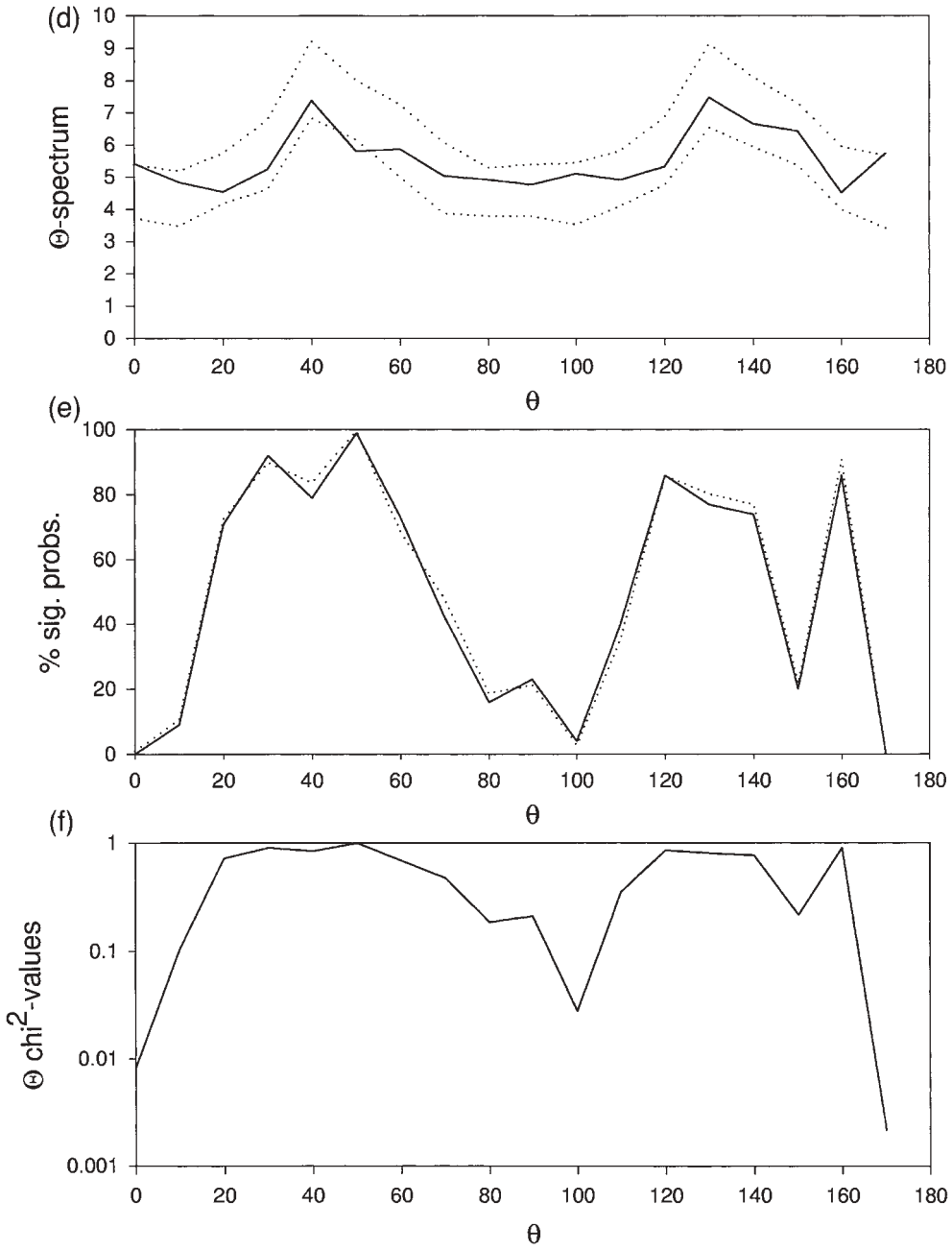

Fig. 6. Point R-spectrum analyses ($r = 1, \ldots, 40$) showing: (a) percentage contribution to overall variance (——) and upper and lower envelopes based on 99 randomisations (· · · · · ·), (b) percentage χ^2 significance probabilities (· · · · · ·) and 100−rank (——), and (c) ln of χ^2 significance probabilities (truncated at 10^{-5}); (d)–(f) show corresponding figures for the point Θ-spectrum

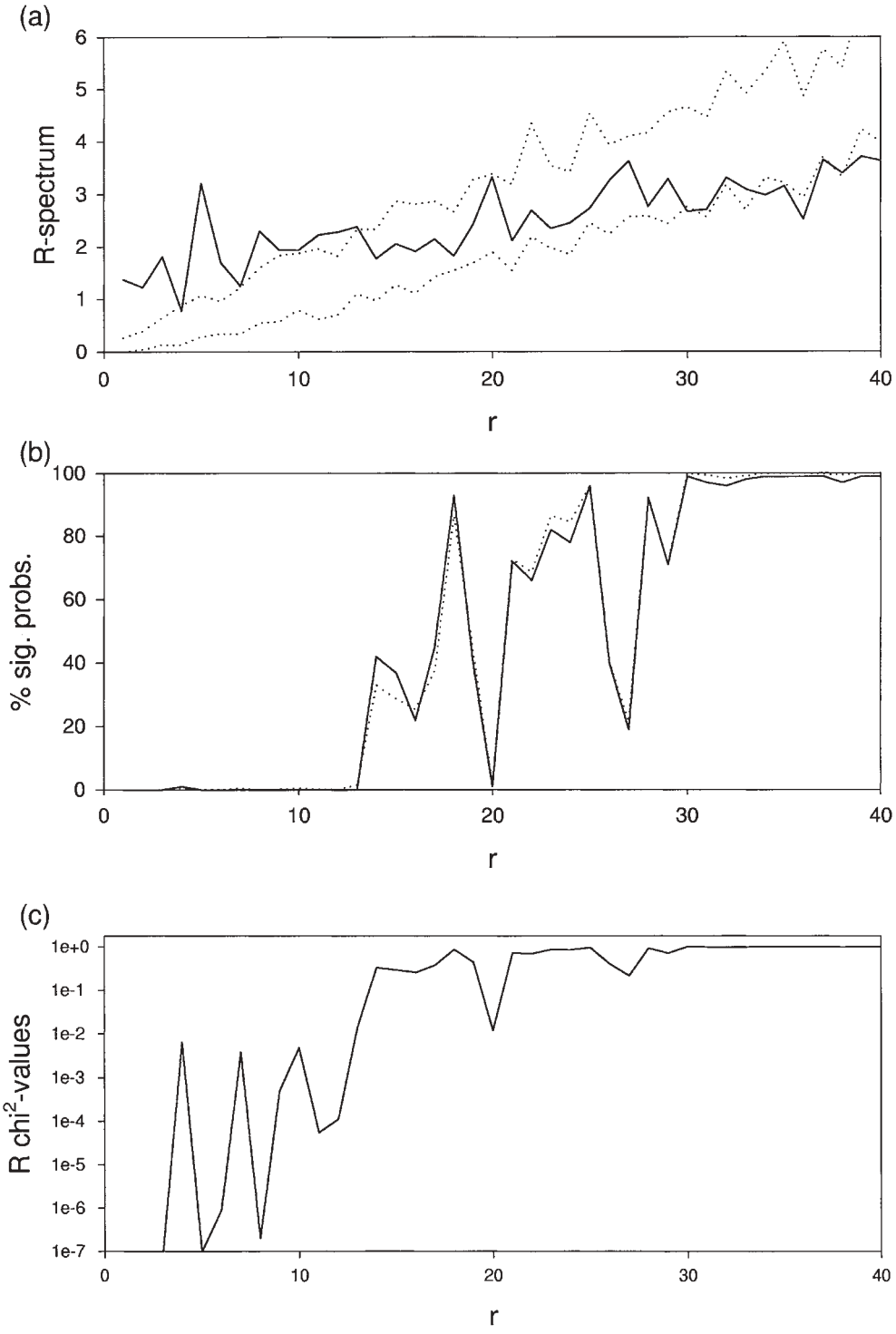
(a)
R-spectrum
0
1
2
3
4
5
6
0
10
20
30
40
r
(b)
% sig. probs.
0
20
40
60
80
100
0
10
20
30
40
r
(c)
R chi^2-values
1e+0
1e-1
1e-2
1e-3
1e-4
1e-5
1e-6
1e-7
0
10
20
30
40
r

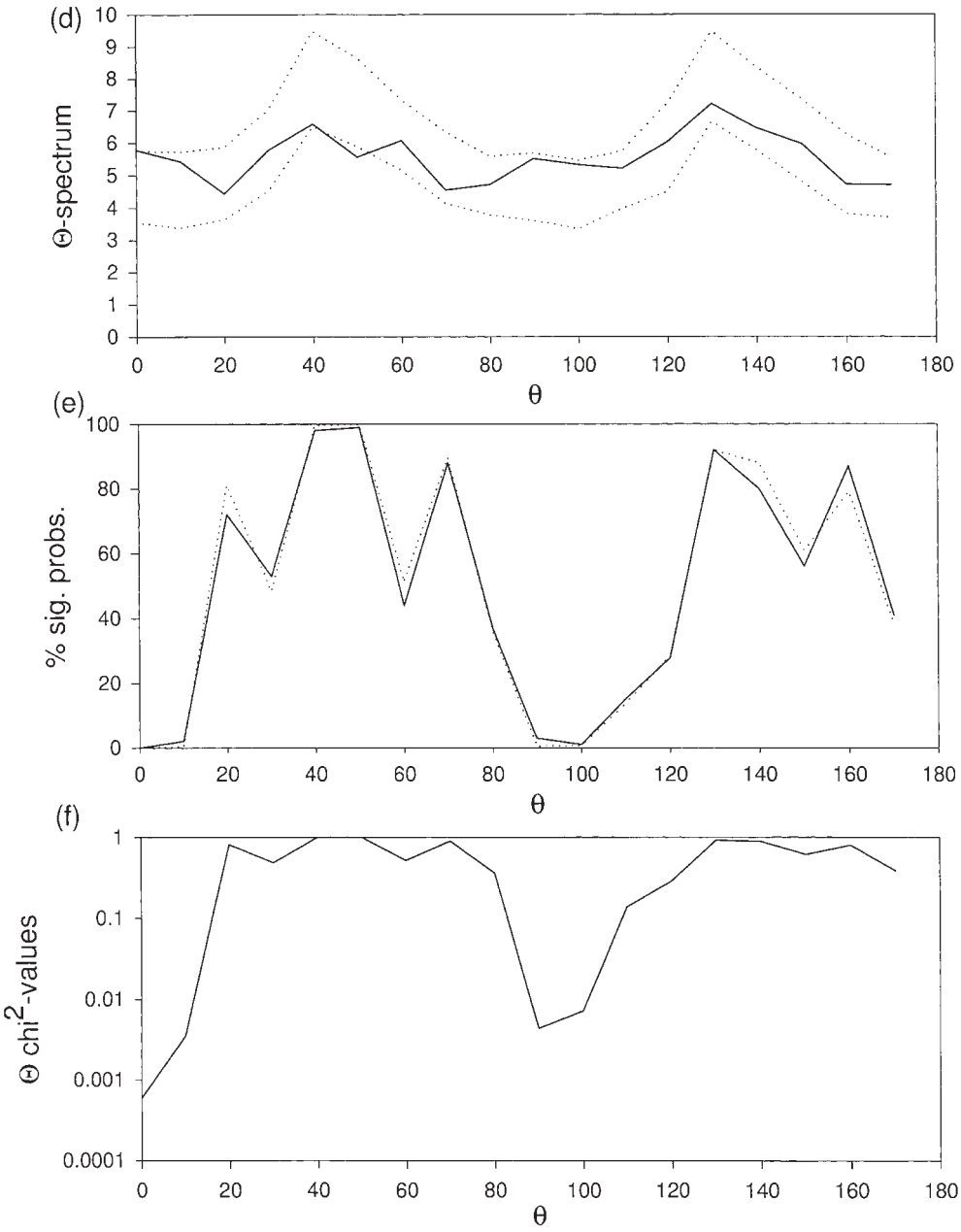

Fig. 7. Mark R-spectrum analyses ($r = 1, \ldots, 40$) showing: (a) percentage contribution to overall variance (——) and upper and lower envelopes based on 99 mark randomisations over the pine locations (·····), (b) percentage χ^2 significance probabilities (·····) and 100−rank (——), and (c) ln of χ^2 significance probabilities (truncated at 10^{-7}); (d)–(f) show corresponding figures for the mark Θ-spectrum

not only highlights this structure, but that it also provides an associated significance probability.

STOYAN and STOYAN (1996) provide a compelling space-domain analysis of these data based on the clear premise that in this forest trees appear in clusters, in common with other natural pine stands (GAVRIKOV, GRABARNIK, and STOYAN, 1993; PENTTINEN, STOYAN, and HENTTONEN, 1992). First, they note that attempts to fit a Neyman-Scott cluster process were not particularly successful. For the empirical $L(r)$-function

$$L(r) = \sqrt{K(r)/\pi} \tag{5.2}$$

does not show the behaviour expected since $\hat{L}(r) - r$ does not tend to zero as $r \to \infty$, as required. This leads them to develop a generalised version of this process, in which two types of clusters, small and large, are allowed (as is clearly apparent in Figure 4) which does yield an acceptable fit to the data.

A similar analysis for the mark periodogram $\{I^M_{pq}\}$ (Figure 5b), based on (2.11) and (2.12), shows surprisingly high agreement with the point process analysis, suggesting that it is the tree locations themselves, rather than their diameters, that form the main component of spatial pattern. Figures 7a, 7b and 7c verify that (like the point spectra) low R-values for $r \leq 12$ are strongly significant, being highly indicative of clustering. Note that the row and column directional effects are also present (Figures 7d, 7e and 7f), though the null hypothesis of isotropy is now rejected much more strongly. It would be interesting to try and obtain greater understanding of the biological process involved here.

Given that the mark spectrum depends on both marks **and** points, and that a substantial amount of point structure is clearly present (Figure 6), the question arises as to whether it is reasonable to base inferences on mark spatial structure on the χ^2-measure. A parallel randomisation procedure to that applied to the points was therefore implemented, with the marks being randomly allocated to the (fixed) tree locations. Any difference between the χ^2 and randomisation approaches therefore reflects the difference between the joint mark-point spectrum and the conditional mark|point spectrum. Not only do the R- and Θ-envelopes based on the 99 randomisations (Figures 7a and 7d) agree with the above mark-point χ^2 results, but the χ^2 and 100-rank plots are in almost exact agreement with each other. So for these longleaf pine data, the marks provide no extra scales of pattern, but simply strengthen the inferences made from the pure point pattern. This is perfectly reasonable, since it is known that the Wade Tract is relatively free of human disturbance, and so remains unaffected by (for example) thinning strategies that might be imposed on managed woodland based on say tree volume and nearest-neighbour differences. The main mark generating process will therefore be local competition for resource, with isolated trees having greater potential for growth than trees growing in tight clusters. This was verified by a subsequent space domain analysis showing evidence of a positive association between marks and nearest-neighbour marks, combined with evidence that high marks are associated with large nearest-neighbour distances.

To conclude, we stress that the spectral approach provides an additional method of spatial analysis, and not a replacement for established distance-based approaches. Its great attraction is that being based on the Fourier coefficients, and hence on a 1–1 transformation of the data, it is not affected by any prior judgement on the form of possible spatial structure. As such, it provides an excellent first attack for the analysis of spatial data sets; any likely spatial structure highlighted can then be studied further through more specific space-domain approaches (as illustrated by the two-type cluster model of STOYAN and STOYAN, 1996).

References

BARTLETT, M. S., 1963: The spectral analysis of point processes (with Discussion). *J. Roy. Statist. Soc.* B **25**, 264–296.

BARTLETT, M. S., 1964: The spectral analysis of two-dimensional point processes. *Biometrika* **51**, 299–311.

BRILLINGER, D. R., 1972: The spectral analysis of stationary interval functions. *Proc. 6th Berkeley Symp. on Math. Stats. and Prob.* **1**, 483–513.

CAPOBIANCO, R. and RENSHAW, E., 1998: The autocovariance function for marked point processes: a comparison between two different approaches. *Biometrical Journal* **40**, 1–16.

CHANDLER, R. E., 1995: A spectral method for estimating parameters in rainfall models. Technical Report No. 142. University College, London.

COX, D. R. and ISHAM, V., 1980: *Point Processes*. Chapman and Hall, London.

COX, D. R. and LEWIS, P. A. W., 1966: *The Statistical Analysis of Series of Events*. Methuen, London.

CRESSIE, N. A. C., 1993: *Statistics for Spatial Data* (revised edition). Wiley, New York.

DALEY, D. J. and VERE-JONES, D., 1972: A summary of the theory of point processes. In *Stochastic Point Processes* (LEWIS, P. A. W. (ed.), pp. 299–383). Wiley, New York.

DALEY, D. J. and VERE-JONES, D., 1988: *An Introduction to the Theory of Point Processes*. Springer-Verlag, Berlin.

DIGGLE, P. J., 1981: Binary mosaics and the spatial pattern of heather. *Biometrics* **37**, 531–539.

DIGGLE, P. J., 1983: *Statistical Analysis of Spatial Point Patterns*. Academic Press, London.

FIKSEL, T., 1988: Edge-corrected density estimators for point processes. *Statistics* **19**, 67–75.

FORD, E. D. and RENSHAW, E., 1984: The interpretation of process from pattern using two-dimensional spectral analysis: modelling single species patterns in vegetation. *Vegetatio* **56**, 113–123.

GAVRIKOV, V. L., GRABARNIK, P. and STOYAN, D., 1993: Trunk-top relations in a Siberian pine forest. *Biometrical Journal* **35**, 487–498.

GOULARD, M., GRABARNIK, P. and SÄRKKÄ, A., 1996: Parameter estimation for marked Gibbs processes through maximum pseudo-likelihood method. *Scandinavian Journal of Statistics* **23**, 365–379.

HANISCH, K.-H. and STOYAN, D., 1979: Formulas for the second-order analysis of marked point processes. *Math. Operationsforach. Statist. Ser. Statistics* **10**, 555–560.

LEWIS, P. A. W., 1972: Recent results in the statistical analysis of univariate point processes. In *Stochastic Point Processes* (LEWIS, P. A. W. (ed.), pp. 1–54). Wiley, New York.

MUGGLESTONE, M. A. and RENSHAW, E., 1996: A practical guide to the spectral analysis of spatial point processes. *Computational Statistics and Data Analysis* **21**, 43–65.

MUGGLESTONE, M. A. and RENSHAW, E., 2001: Spectral tests for randomness for spatial point patterns *Environmental and Ecological Statistics* **8**, 237–251.

NEWBERY, D. MCC., RENSHAW, E. and BRUNIG, E. F., 1986: Spatial pattern of trees in Kerangas Forest, Sarawak. *Vegetatio* **65**, 77–89.

NEYMAN, J. and SCOTT, E. L., 1958: Statistical approach to problems of cosmology (with Discussion). *J. Roy. Statist. Soc.* B **20**, 1–43.

OGATA, Y., IMOTO, M. and KATSURA, K., 1991: 3-D spatial variation of *b*-values of magnitude-frequency distribution beneath the Kanto District, Japan. *Geophys. J. Int.* **104**, 135–146.

OGATA, Y. and KATSURA, K., 1988: Likelihood analysis of spatial inhomogeneity for marked point patterns. *Ann. Inst. Statist. Math.* **40**, 29–39.

OGATA, Y. and KATSURA, K., 1993: Analysis of temporal and spatial heterogeneity of magnitude frequency distribution inferred from earthquake catalogues. *Geophys. J. Int.* **113**, 727–738.

OGATA, Y. and TANEMURA, M., 1985: Estimation of interaction potentials of marked spatial point patterns through the maximum likelihood method. *Biometrics* **41**, 421–433.

OHSER, J. and STOYAN, D., 1981: On the second-order and orientation analysis of planar stationary point processes. *Biometrical Journal* **23**, 523–533.

PENTINNEN, A., STOYAN, D., and HENTTONEN, H. M., 1992: Marked point processes in forest statistics. *Forest Science* **38**, 806–824.

PLATT, W. J., EVANS, G. W., and RATHBUN, S. L., 1988: The population dynamics of a long-lived conifer (*Pinus palustris*). *American Naturalist* **131**, 491–525.

PRIESTLEY, M. B., 1964: The analysis of two-dimensional stationary processes with discontinuous spectra. *Biometrika* **51**, 195–217.

PRIESTLEY, M. B., 1981: *Spectral Analysis and Time Series. Vol. 1: Univariate Series*. Academic Press, London.

RATHBUN, S. L. and CRESSIE, N., 1990: A space-time survival point process for a longleaf pine forest in southern Georgia. Statistical laboratory preprint No. 90–13, Iowa State University, Ames, IA.

RENSHAW, E., 1984: Competition experiments for light in a plant monoculture: an analysis based on two-dimensional spectra. *Biometrics* **40**, 717–728.

RENSHAW, E. and FORD, E. D., 1983: The interpretation of process from pattern using two-dimensional spectral analysis: methods and problems of interpretation. *Appl. Statist.* **32**, 51–63.

RENSHAW, E. and FORD, E. D., 1984: The description of spatial pattern using two-dimensional spectral analysis. *Vegetatio* **56**, 75–85.

RENSHAW, E., PHAYRE, S., and JAKEMAN, E., 2000: The development of space-time interaction processes with given spectral structure. *Inverse Problems* **16**, 877–890.

RENSHAW, E. and SÄRKKÄ, A., 2001: Gibbs point processes for studying the development of spatial-temporal stochastic processes. *Computational Statistics and Data Analysis* **36**, 85–105.

RIPLEY, B. D., 1976: The second-order analysis of stationary point processes. *J. Appl. Prob.* **13**, 255–266.

STOYAN, D., 1984a: On correlations of marked point processes. *Math. Nachr.* **116**, 197–207.

STOYAN, D., 1984b: Correlations of the marks of marked point processes – statistical inference and simple models. *Elektron. Informationsverarb. u. Kybernet*. **20**, 5/6, 285–294 (Journal of Information Processing and Cybernetics).

STOYAN, D., 1992: Statistical estimation of model parameters of planar Neyman-Scott cluster processes. *Metrika* **39**, 67–74.

STOYAN, D., KENDALL, W. S., and MECKE, J., 1987: *Stochastic Geometry and Its Applications*. Wiley, New York.

STOYAN, D. and STOYAN, H., 1994: *Fractals, Random Shapes and Point Fields: Methods of Geometrical Statistics*. Wiley, New York.

STOYAN, D. and STOYAN, H., 1996: Estimating pair correlation functions of planar cluster processes. *Biometrical Journal* **38**, 259–271.

THOMAS, M., 1949: A generalization of Poisson's binomial limit for use in ecology. *Biometrika* **36**, 18–25.

WATSON, G. N., 1944: *A Treatise on the Theory of Bessel Functions* (2nd edition). Cambridge University Press.

Received, May 2001
Revised, January 2002
Accepted, January 2002